# Journal of Materials Chemistry A



View Journal

View Article Online

## PAPER



Cite this: DOI: 10.1039/d5ta05588a

# A printable asymmetrical surface pattern for responsive directional liquid transport

Yi Zhang, abc Danfeng Pei, abc Mingjie Liabc and Chaoxu Li \*\* \*\* Liabc \*\* L

Long-distance directional liquid surface transport is of great importance not only for many biologic functionalities of living organisms, but also for broad applications of open-channel microfluidics, microreactors, heat transfer, water harvesting, and chemo/bioanalysis. However, relevant studies have long concentrated on asymmetric 3D arrays produced by complicated microfabrication techniques. Also, it remains challenging to switch the liquid surface transport direction on demand in a specific system. Herein, we showed that directional liquid transport could be controlled easily on printable asymmetric surface patterns *via* anisotropic interactions between the topographical barriers and the liquid. Due to the unbalanced motion resistance and Laplace pressure, liquids showed different directional transport modes according to their surface tension. When patterned on elastic substrates, mechanical stretching could change their characteristic geometric parameters and thereby switch the direction of liquid transport. Thus, this study may not only offer an affordable and ingenious surface that can achieve liquid directional steering dictated by its inherent properties, but also pose an endurable and simple method for intelligent liquid transport control. The responsiveness to liquids and strains offered extra flexibility of switching liquid transport directions essential in liquid droplet separation and open-channel microfluidics.

Received 11th July 2025 Accepted 22nd October 2025

DOI: 10.1039/d5ta05588a

rsc.li/materials-a

#### Introduction

Directional liquid transport is not only of great importance for many biologic functionalities of living organisms (e.g., fog/water collection for cactus thorns, lubrication for the peristome of N. alata and water out-guidance for wings of M. deidamia), 1-5 but also being pursued for applications in open-channel microfluidics,6 microreactors,7,8 heat transfer,9 water harvesting,10 and chemo/bioanalysis.11,12 To achieve spontaneous directional liquid transport, different chemical gradients (e.g., in wettability and stiffness) and asymmetric topographies (e.g., in curvature, shape and array arrangements) have been designed for unbalanced capillary forces, Laplace pressure and pinning effects. 13-16 In contrast to the limited transport distance available for spatial chemical gradients, asymmetric surface topographies showed great potential for practical applications due to their relevance to biologic systems and superiority in longdistance liquid transport.<sup>17</sup> Various biological and artificial asymmetric topographies have been investigated to achieve unidirectional liquid surface transport. 17-19 Besides the cone-/ spindle-like fibers with curvature gradients,20 relevant studies concentrated mainly on three-dimensional (3D) tilted micrometric arrays on planar surfaces produced by complicated microfabrication techniques (*e.g.*, replica molding,<sup>21</sup> laser ablation,<sup>22</sup> and digital light processing<sup>23</sup>). Also, it remains challenging to switch the liquid surface transport direction on demand in a specific system.

By constructing tilted micro-pit arrays on conical spines, oil droplets were found to be transported from the spine tips to their base sides due to unbalanced Laplace pressure.24 Mimicking the Araucaria leaf, 3D arrays of tilted micro-ratchets were also designed on surfaces.25 It was found that the asymmetric reentrant effect enabled liquid transport along the ratchet-tilting direction for low-surface-tension liquid transport and along the opposite direction for high-surface-tension liquids. Yang further produced asymmetric reentrant microarrays by mimicking Crassula muscosa leaves by 3D printing.19 By varying the tilting reentrant angles, ethanol could be transported unidirectionally in either direction due to the heterogeneous liquid meniscus. By incorporating magnetic fillers into the reentrant arrays, the magnetic field could even switch the liquid transport direction by changing the reentrant angles. Analogously, the asymmetric re-entrant structure was further optimized by Zhou to reinforce the tendency of unidirectional liquid transport.26 By combining the magneto-responsive wires and surface superhydrophobic treatment, the impact dynamic control and selective transport of droplets, precise object manipulation and chemical reactions are demonstrated. 27,28 These 3D microarrays on planar surfaces promised great

<sup>&</sup>quot;Group of Biomimetic Smart Materials, CAS Key Laboratory of Bio-Based Materials, Qingdao Institute of Bioenergy and Bioprocess Technology, Chinese Academy of Sciences, Songling Road 189, Qingdao 266101, P. R. China. E-mail: licx@qibebt.ac.cn bShandong Energy Institute, Songling Road 189, Qingdao, China

<sup>&</sup>lt;sup>4</sup>Cingdao New Energy Shandong Laboratory, Songling Road 189, Qingdao, China <sup>4</sup>Center of Material and Optoelectronics Engineering, University of Chinese Academy of Sciences, 19A Yuquan Road, Beijing 100049, P. R. China

potential to control liquid flow for open-channel microfluidic systems. But their topographical complexities normally relied on high-cost, time-consuming and sophisticated microfabrication processes. Their structural fragility also reduced their mechanical endurance and service life.

Besides 3D arrays, sub-millimetric hydrophilic channels containing asymmetric superhydrophobic barriers inside were recently generated on glass substrates through fluorination and photocatalytic irradiation in the presence of photomasks.<sup>29</sup> It was found that the unbalanced capillary forces could drive water transport along one direction, whereas it was pinned at the other side. Within similar open channels containing hydrophobic barriers inside, manipulation of the water transport direction could also be achieved by adjusting the wettability of channel sidewalls.<sup>30</sup>

In contrast to these complicated 3D structures and manufacturing process, direct writing/printing 2D patterns may provide a low-cost and endurable solution for open-channel microfluidic systems. Herein we designed a millimetric 2D Vshape structure within parallel sidelines through direct writing without any physical or chemical post-treatment. It was found that the combination of unbalanced motion resistance and Laplace pressure could drive directional liquid transport. That is, a low-surface-tension liquid favored the tip-oriented direction, and a high-surface-tension liquid favored the opposite direction. Even for a specific liquid, above 50% strain of elastic substrates could switch the liquid transport direction due to the varying geometric parameters of the V-shaped structure. Moreover, the intelligent response capability allows the functional surface to be an automatic liquid separator. In contrast to the complicated 3D tilted arrays and their sophisticated microfabrication techniques, the endurable 2D V-shape structure and simple fabrication method will offer a promising solution for building portable and cost effective open microfluidic surfaces for long-distance liquid directional steering. The responsiveness to liquids and strain further offers the extra flexibility of controlling liquid transport directions essential in open-channel microfluidics.

#### Results and discussion

#### Patterned surfaces and liquid-responsive directional transport

The millimetric V-shape structure within parallel sidelines was fabricated via a commercial direct-ink-writing (DIW) printer as shown in Fig. 1A. Fluidic prepolymer of silicone was written on glass substrates along the predetermined path for further solidification. The same V letters (with a width  $D \sim 3$  mm, a tilting angle  $\alpha \sim 20^\circ$  and a radius of vertex curvature  $R \sim 150$  µm) were written sequentially with an interval distance of 4 mm within two parallel sidelines (with a width  $W \sim 3.5$  mm between adjacent sidelines, Fig. 1B). The transverse gaps between the V letter and the adjacent sidelines remained the same on both sides (with the gap width d = (W - D)/2-250 µm). The silicone lines were approximately semicircular in cross section and  $\sim 160$  µm in height h and 300 µm in width w (Fig. 1C). The geometric parameters of the V patterns (i.e., tilting angle  $\alpha$ , width D and vertex radius R) were tuned to control the liquid

transport direction. The V vertex direction was labeled as +s, and the opposite direction was labeled as -s.

When pumping the liquid continuously between the adjacent V letters at a constant rate of 10  $\mu$ L s<sup>-1</sup>, three modes of liquid transport behavior are exhibited on the patterned surface due to liquid surface tension (Fig. 1D and Movie S1). The unidirectional transport behavior of the liquids was evaluated based on the distances of liquid transport in both directions (*i.e.*,  $L_{+s}$  and  $L_{-s}$ ). On a patterned glass substrate with the typical silicone V shape (*i.e.*, geometric parameter  $\alpha=20^\circ$ ,  $d=250~\mu$ m and  $R=150~\mu$ m), it was found that the unidirectional liquid transport ability depended strongly on the liquid inherent properties.

For a liquid with a low surface tension of 20.9 mN m $^{-1}$  (e.g., isopropyl alcohol), symmetric transport towards both the opposite directions was observed along the sidewalls (symmetric transport mode, Fig. 1D(i) and E). The liquids with higher surface tension were obtained by progressively adding water to ethanol. As shown in Fig. S1, the liquid surface tension could increase from 21.8 mN m $^{-1}$  (pure ethanol) to 72.1 mN m $^{-1}$  (pure water). For the liquid with 21.8–23.6 mN m $^{-1}$  surface tension (i.e., percentage of water ranges from 0 to 25 wt%), the liquid transported preferentially towards the +s direction (+s directional transport mode, Fig. 1D(ii) and E), and there may occur a slight backflow at the early stage (Fig. 1F).

For a liquid with 25.2–34.1 mN m<sup>-1</sup> surface tension (percentage of water ranges from 30 to 70 wt%), the liquid transported preferentially towards the –s direction (–s directional transport mode, Fig. 1D(iii)). The transport process in the –s direction was discontinuous due to the apparently temporary liquid accumulation and then onrush at the V vertex barriers. For the liquid with > 39 mN m<sup>-1</sup> surface tension (percentage of water exceeds 80 wt%), there was no liquid spreading analogous to the dewetting behavior on solid substrates. Continuous liquid pumping on the patterned surfaces would result in extra accumulation and effusion over the sidelines (Fig. S2). As shown in Fig. S3, the durability of the surface has been further verified, and the unidirectional transmission of liquid can still remain stable after 100 repetitive experiments.

#### Symmetric transport for low-surface-tension liquid

To explain the mechanisms responsible for the liquid directional transport mode regulation, we first investigate the differences in spreading behaviors of various liquids passing through the gap between the V letter and the adjacent sidelines. When a liquid met a micrometric gap, as modeled in the inset image M–M of Fig. 2A, spontaneous capillary flow occurs when the generalized Cassie angle  $\theta^*$  is smaller than  $\pi/2$ , and becomes:  $^{31,32}$ 

$$\cos \theta^* = \sum_{i} (\cos \theta_i f_i) = 0.189 \cos \theta_1 + 0.381 \cos \theta_2 - 0.432 > 0$$

(1)

where  $\theta_i$  and  $f_i$  are Young's contact angle with each interface and the fractional area of each component in a cross section of the

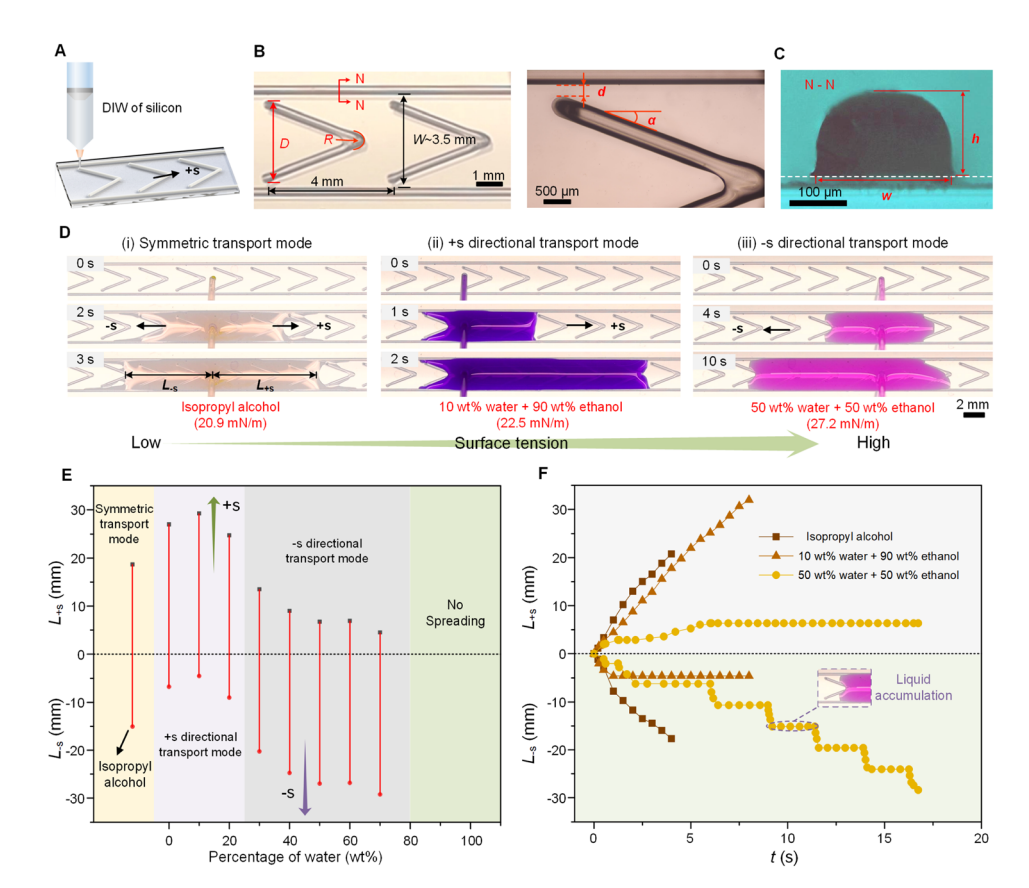


Fig. 1 Three liquid transport modes based on the surface tension of the liquid. (A) Schematic illustration of the direct ink writing process. (B) Typical geometric parameters of the surface pattern. The distance of the adjacent V pattern and parallel sidelines is 4 mm and 3.5 mm, respectively. The width D, radius of vertex curvature R and tilting angle  $\alpha$  can be varied. (C) Cross-sectional view of the silicone line. The height h and width w of the silicone line are 160 µm and 300 µm, respectively. (D) Varying liquids with different surface tensions in (i) symmetric transport mode, (ii) +s directional transport mode and (iii) -s directional transport mode. (E) Three modes of liquid transport identified based on liquid transport distances ( $L_{+s}$  and  $L_{-s}$ ) along two directions and liquids of different water compositions in ethanol. (F) Temporal variation of  $L_{+s}$  and  $L_{-s}$ in three modes of liquid transport. The inset image shows temporary liquid accumulation before onrush at the V vertex.

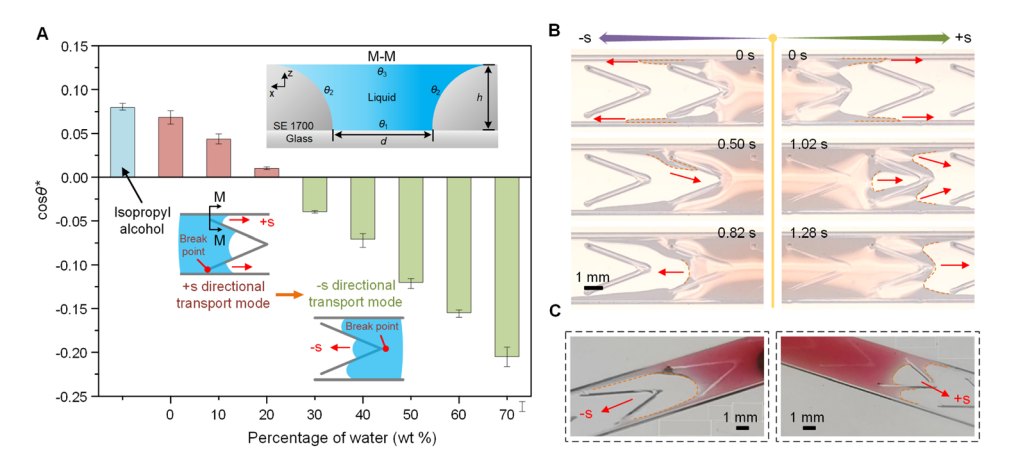


Fig. 2 Symmetric transport for a low-surface-tension liquid. (A) Generalized Cassie angle  $\theta^*$  for spontaneous capillary flow for liquids of different water compositions in ethanol. The inset M-M illustrates cross-sectional morphology of liquid in the gap between the V letter and the adjacent sidelines of silicone. Liquids preferentially pass through the narrow gap during the transport process when  $\cos\theta^* > 0$ . With the increase in liquid surface tension, the break point is transformed from the gap on the sides to the vertex of the V letter. (B) Spreading dynamics of symmetric transport of isopropyl alcohol as a low-surface-tension liquid. Isopropyl alcohol spreads along the sidelines in two directions and visible capillary filaments ahead of bulk flow are formed. (C) Oblique view of the morphology of the isopropanol concave meniscus in two directions.

flow (containing the interface between the liquid and glass bottom  $f_1 = d/(2h + 2d + \pi h) = 0.189$ ; the interface between the liquid and silicone lines  $f_2 = \pi h/(2h + 2d + \pi h) = 0.381$ ; and the interface between the liquid and air  $f_3 = (2h + d)/(2h + 2d + \pi h) = 0.432$ . Here, the contact line between the liquid and the silicone lines is considered a quarter arc and the interface between liquid and vapor is often regarded as a hydrophobic surface with a contact angle  $\theta_3$  of 180°.

When the generalized Cassie angle  $\theta^*$  is smaller than  $\pi/2$ (general condition for the spontaneous capillary flow in a composite channel being satisfied31), liquids preferentially pass through the narrow gap during the transport process (symmetric transport mode or +s directional transport mode). When increasing the water composition in the mixture for a larger surface tension and contact angle of liquids, the generalized Cassie angle ( $\cos \theta^*$ ) for spontaneous capillary flow turned from positive to negative, resulting in the transition from the driving force to resistance for liquids passing through the gap. The break points are transformed from the gap on sides to the vertex of the V letter and the liquid transport direction is also reversed (-s directional transport mode, Fig. 2A). For a lowsurface-tension liquid such as isopropyl alcohol, the low contact angles at the liquid/solid interfaces (e.g., 1° for glass and 21° for silicone) gave  $\cos \theta^* > 0$ . This implied the overwhelming interfacial forces at the liquid/solid interfaces and led to spontaneous liquid transport through the narrow gap, analogous to the spontaneous wetting behavior on solid substrates. In the case of liquid transport along silicone V-shape structures within parallel sidelines on glass (Fig. 2B), the liquid could easily pass through the narrow gaps between the V pattern and sidelines in both the +s and -s directions due to the capillary force and corner effect formed by the silicone line pattern and substrate, and the impact of the V pattern is almost negligible. In the +s direction, liquid preferentially transported along the sidelines (see the 0 s photograph in Fig. 2B) and may form the middle void space within the V-shape structures (see the 1.02 s photograph in Fig. 2B and C). With continuous liquid accumulation, the liquid gradually filled the void, and then combined with the bilateral liquid along the sidelines (see the 1.28 s photograph in Fig. 2B). In the -s direction, liquid was transported preferentially through the narrow gaps and then may be hindered by the V-shaped pattern, and the backflow along the inner lines caused the intermediate liquid to continue flowing backward over the barrier (see the 0.50 s and 0.82 s photograph in Fig. 2B). The advancing meniscus of liquid remained concave in shape throughout the entire liquid transfer process (Fig. 2C).

#### Unidirectional liquid transport in the +s direction

On increasing the surface tension of liquid and thereby the contact angles on the interfaces between the liquid and the solid, the resistance of silicone lines to liquid transport would start to become apparent. For the liquid of ethanol containing 10 wt% water, in the +s direction, liquid transport was initially hindered by the side tails of the V pattern and formed a convex liquid meniscus (see the 0.08 s photograph in Fig. 3A), which then transformed into a concave surface (see the 0.16 s

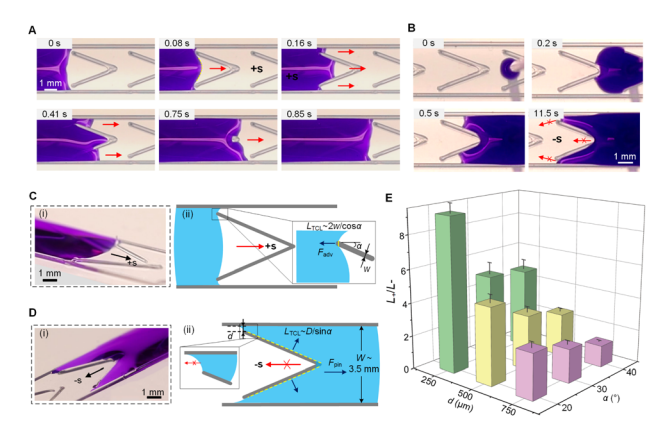


Fig. 3 Unidirectional liquid transport in the +s direction. (A) Spreading dynamics of the liquid along the +s direction. Liquid filled the middle void space within the V letter preferentially, and then passed through the narrow gaps until it covered the entire pattern. (B) Pinning dynamics of a liquid in the -s direction. (C) The morphology of the liquid precursor after contact with the side tails of the V-shaped pattern in the +s direction and schematic illustration of the TCL. (D) Pinning state in the -s direction and schematic illustration of the TCL. Liquid flow is blocked at the junction due to the fluidic diode effect. (E) Correlation of the transport distance ratio  $(L_{+s}/L_{-s})$  of liquid along two directions with geometric parameters of the V letter. The unidirectional liquid transport ability decreases with the increase in gap width d and barrier tilting angles  $\alpha$ . Liquid: ethanol containing 10 wt% water.

photograph in Fig. 3A). Compared with isopropyl alcohol, the capillary filaments ahead of bulk flow are not prominent due to the decrease in wettability. The liquid preferentially filled the middle void space within the V letter before passing through the narrow gaps between the V pattern and sidelines (see the 0.41 s photograph in Fig. 3A and S4). In the —s direction, liquid transport was hindered by the silicone V line (see the 0.5 s photograph in Fig. 3B). The abrupt cross-section changes from wide channels to narrow channels would lead to a fluidic diode effect, 33,34 which may obstruct liquid transport through the narrow gaps between the V pattern and sidelines (see the 11.5 s photograph in Fig. 3B).

As shown in Fig. 3C and D, liquid transport was governed by the competing resistance between the side tails of the V pattern in the +s direction (Fig. 3C(i)) and the profile line of the V pattern in the –s direction (Fig. 3D(i)). Due to the low height of the silicone line, we simplified the V-shaped pattern as a 2D hydrophobic water barrier. Following the contact between the liquid precursor and V pattern in the +s direction, the silicone barrier stabbed into the liquid film in a nearly perpendicular way, and the three-phase contact line (TCL) length was described with the width w (300  $\mu$ m) of the silicone line as  $2w/\cos\alpha$  (Fig. 3C(ii)). And the interfacial TCL resistance was expressed as:<sup>35</sup>

$$F_{+s} = 2 \cdot w \cdot \gamma \cdot (\cos \theta - \cos \theta_{e}) / \cos \alpha \tag{2}$$

where  $\gamma$  is the surface tension of liquid,  $\cos \theta$  and  $\cos \theta_e$  were the real-time contact angle and equilibrium contact angle, respectively. In the -s direction, the TCL length along the V-letter was

expressed as  $(W - 2d)/\sin \alpha$ . And the interfacial TCL resistance along the axial direction was expressed as:

$$F_{-s} = (W - 2d) \cdot \gamma \cdot (\cos \theta - \cos \theta_{e}) \tag{3}$$

The competition between the interfacial TCL resistances of the opposite directions could be estimated by using:

$$F_{-s}/F_{+s} = (W - 2d) \cdot \cos \alpha/2w \tag{4}$$

That is, the unidirectional transport ability of a liquid towards the +s direction depended on geometric parameters of the V patterns (i.e., tilting angle  $\alpha$  and gap width d), when fixing a width W of 3.5 mm between two adjacent parallel sidelines and silicone line width w of 300 µm (Fig. S5).

Accordingly, the small angle  $\alpha$  and gap width d of V patterns tended to increase the  $F_{-s}/F_{+s}$  value, and led to a larger motion resistance for liquid transport in the -s direction. For example,  $F_{-\rm s}/F_{+\rm s}\sim$  4.5 was obtained for  $\alpha=20^{\circ},\, d=250$  µm. In the +s direction, the liquid of ethanol containing 10 wt% water formed the concave liquid front and thereby the Laplace pressure towards the +s direction. The liquid would preferentially be transported through the narrow gap between the V letter and sidelines. When evaluating the unidirectional liquid transport by using the distance ratio  $(L_{+s}/L_{-s})$  of liquid transport, it was found that the large  $L_{+s}/L_{-s}$  value was favored by the small d value and  $\alpha$  (Fig. 3E), being consistent with the  $F_{-s}/F_{+s}$  value. It is to be noted that the large liquid pumping rates may depress the tendency of unidirectional liquid transport due to possible liquid overflow in the opposite direction. When the pinning state collapses, liquid effused from the vertex of the V-letter due

to the Laplace pressure caused by the concave liquid front (Fig. S6A). Hence, the unidirectional liquid transport ability could be improved by increasing the vertex radius R without changing other channel parameters. Compared to  $R \sim 150 \mu m$ , the distance ratio  $(L_{+s}/L_{-s})$  increased by more than 100% for the channel with  $R \sim 300 \, \mu \text{m}$  (injection velocity: 50  $\mu \text{L s}^{-1}$ , Fig. S6B).

#### Unidirectional liquid transport in the -s direction

As the water content of the liquid increases from 10 wt% to 50 wt%, it had large surface tension ( $\sim$ 27 mN m<sup>-1</sup>) and contact angles on the solid interfaces ( $\sim 15^{\circ}$  for glass substrates;  $\sim 62^{\circ}$ for silicone lines). The silicone lines in both directions exerted large interfacial resistances to liquid transport and the Cassie angle for spontaneous capillary flow  $\cos \theta^* < 0$ . Therefore, liquids cannot pass through the gap spontaneously. In the -sdirection, the silicone lines also posed the interfacial TCL resistance to liquid transport (Fig. 4A). However, as shown in Fig. 4C(i), the liquid would accumulate between the sidelines and give a larger thickness of the liquid layer at the vertex point of V patterns. The liquid accumulation produced a concave liquid front and thereby an additional Laplace pressure  $P_s$ ,  $P_s =$  $\gamma/R_1$ , towards the -s direction that was related to the local radius of the droplet on the vertex point  $(R_1 = w/(1 - \sin \alpha))$ , as shown in Fig. 4C(ii)).28 Thus, the liquid may break the TCL resistances at the vertex point and flow over the vertex in the -sdirection (see the 3.92 s photograph in Fig. 4A). Subsequently, driven by the middle liquid film, the liquid on the sides gradually spread forward until it covered the entire V pattern and filled the next unit at 4.16 s. In the +s direction, liquid transport was hindered by the silicone lines together with the convex

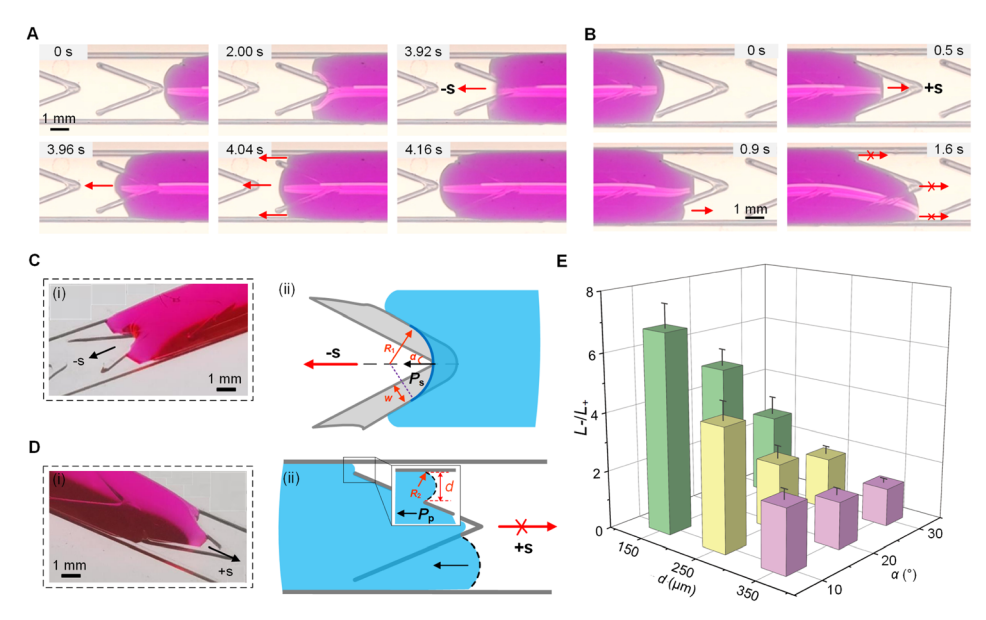


Fig. 4 Unidirectional liquid transport in the -s direction. (A) Spreading dynamics of liquids along the -s direction. A concave surface formed after the contact between the liquid and silicone line, and the liquid crosses the silicone line from the vertex of the V pattern. (B) Spreading dynamics of liquids along the +s direction. (C) Liquid spreading state in the -s direction and schematic illustration of the TCL. (D) Pinning state in the +s direction and schematic illustration of the TCL. Laplace pressure caused by the concave surface  $(P_s)$  and the convex surfaces  $(P_p)$  directed to the -s direction. (E) Dependence of the liquid transport distance ratio  $(L_{-s}/L_{+s})$  on tilting angle  $\alpha$  and gap width d of the V pattern. The unidirectional liquid transport ability decreases with the increase in gap width d and barrier tilting angle  $\alpha$ . Liquid: ethanol containing 50 wt% water.

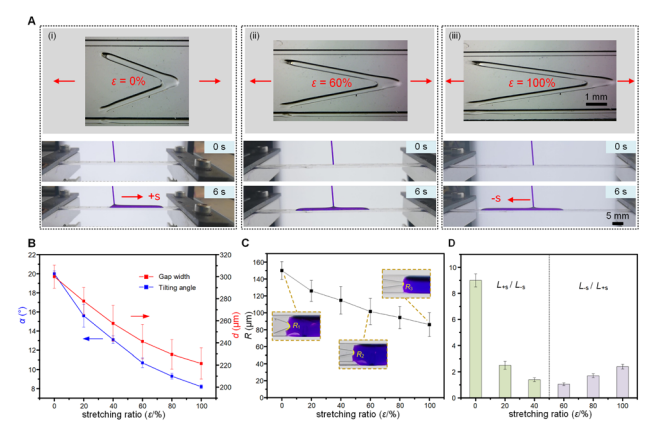


Fig. 5 Strain responsiveness of directional liquid transport. (A) Dependence of liquid transport on the stretching ratio  $(\varepsilon)$  of the elastic substrate. As  $\varepsilon$  increases from 0% to 100%, the liquid transforms from the +s direction to the -s direction. (B) The relationship between the stretching ratio and surface morphology parameters. Gap width d and tilting angle  $\alpha$  decrease with the increase in the surface stretching ratio. (C) Variation of vertex curvature R against the stretching ratio. When the stretching ratio increases from 0% to 100%, the curvature radius R of the liquid film at the vertex decreases from  $\sim$ 150  $\mu$ m to  $\sim$ 86  $\mu$ m. (D) Liquid transport distance ratio at different stretching ratios of the elastic substrate. When the surface stretching ratio exceeds 50%, the liquid transport distance in the -s direction ( $L_{-s}$ ) is greater than that in the +s direction ( $L_{+s}$ ). Liquid: ethanol containing 10 wt% water.

liquid front (Fig. 4B). The convex meniscus of liquid in the narrow gap would produce a Laplace pressure,  $P_{\rm p} = \gamma/R_2$  ( $R_2 \sim d/2$ , Fig. 4D(ii)) towards the  $-{\rm s}$  direction and hinder the liquid transport through the narrow gaps between V letters and sidelines. It is to be noted that liquid overflow cannot be avoided at large liquid pumping rates.

It could be seen that the -s unidirectional transport ability of a liquid with large surface tension was related to the additional Laplace pressure at the vertex point of V letters and narrow gap. Thus, the smaller tilting angle  $\alpha$  may favor the larger Laplace pressure in the -s direction, with other structural parameters remaining the same. In the case of liquid pinning in the +s direction, decreasing the gap width d would generate higher pressure, thereby hindering the liquid transport through the gaps and exhibiting a larger distance ratio (Fig. 4E). As a matter of fact, the transport distance ratio  $L_{-s}/L_{+s}$ 

was found to increase from 2.6 to 10.8 when decreasing the vertex radius R value from 300  $\mu$ m to 100  $\mu$ m with the same gap width and tilting angle (Fig. S7A and S7B).

#### Strain-responsiveness for the direction of liquid transport

For a predetermined liquid, its directional transport depended strongly on the geometric parameters (e.g. gap width d, tilting angle  $\alpha$  and radius of vertex curvature R) of the substrate patterns. When printing the same structure on elastomeric substrates (e.g., PDMS), tensile strains may change the geometric parameters and then the liquid transport directions (Fig. S8). As shown in Fig. 5A, the patterned PDMS substrate (50  $\times$  8 mm<sup>2</sup> in size) was fixed on a tensile stage. At the initial state (0% strain), for the liquid of ethanol containing 10 wt% water, the contact angle ( $\sim$ 21°) gave  $\cos \theta^* > 0$ , causing the liquid to be preferentially transported in the +s direction (Fig. 5A(i), S9A, S10A, and Movie S2). With the increase in the stretching ratio, the transport distance ratio  $(L_{+s}/L_{-s})$  decreased dramatically from 9.1 to 2.5 (20% strain, Fig. 5D). At s strain of 60%, the tilting angle  $\alpha$  and gap width d decreased from  $\sim 20^{\circ}$  and  $\sim 300^{\circ}$  $\mu m$  to  $\sim 10.7^{\circ}$  and  $\sim 241.2 \ \mu m$  (Fig. 5B), together with a smaller vertex radius R (decreased from  $\sim$ 150 µm to  $\sim$ 102 µm, Fig. 5C) and thereby larger additional Laplace pressure in the -s direction (Fig. S10B). The liquid transported nearly symmetrically in both -s and +s directions. At a strain of 100%, the tilting angle  $\alpha$  is only about 8.2°; meanwhile, the curvature radius R of a liquid film at the vertex decreases accordingly, reducing to about half of its initial value (from  $\sim$ 150  $\mu$ m to  $\sim$ 86  $\mu$ m). The Laplace pressure acting on the liquid precursor at the vertex of the V-shape structure increases by approximately two times and leads to liquid transport in the -s direction (Fig. S9C and S10C). In addition, directional liquid transport seemed to be maintained when bending the elastic substrates (e.g., "C" and "S" shaped trajectory in Fig. S11), which offered extra adaptivity for open microfluidic systems.

For the patterned surface with fixed geometric parameters, different liquids could show distinct directional transport behavior (Fig. S12). This phenomenon could be used to isolate droplets of liquids with different surfaces tensions. As depicted in Fig. 6A, the patterned glass substrate was installed on a tiltable platform. And the liquids with different surface tensions were pumped in the middle of the substrate at an appropriate

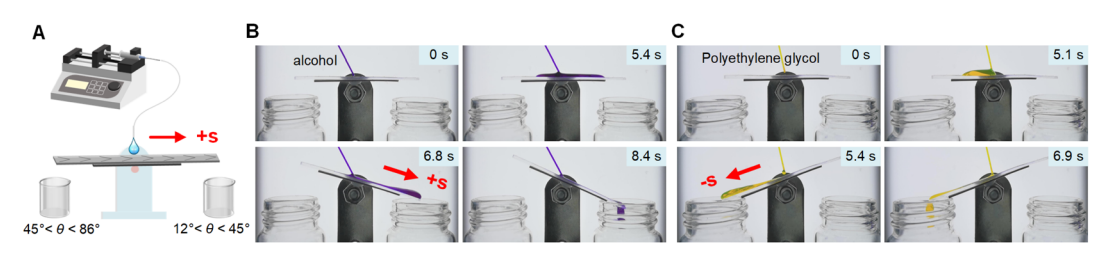


Fig. 6 Isolation of liquids with different surface tensions. (A) Setup of pumping liquids on a tiltable and patterned substrate. Various liquids are injected into the center of the channel with a constant injection velocity of  $10~\mu L~s^{-1}$  and tend to move towards opposite directions due to the differences in wettability, causing the platform to tilt and ultimately be collected in the container. (B) Droplets of alcohol transported in the +s direction on a patterned substrate, were collected by the right container. (C) The collection process of polyethylene glycol containing 85 wt% water on a patterned substrate.

rate. When pumping alcohol on the substrate, the liquid was preferentially transported to the right (Fig. 6B). The substrate tilted to the right and the liquid was collected in the right container. When pumping an aqueous solution of polyethylene glycol (PEG 2000, 15 wt%), the liquid was preferentially transported to the left and collected in the left container (Movie S3).

#### Conclusions

In this study, we showed that directional liquid transport could be controlled easily by using printable asymmetrical surface patterns. A millimetric 2D V-shape structure within parallel sidelines was produced through direct writing. For a fixed pattern with constant geometric parameters, three modes of liquid transport behaviors were identified according to surface tensions of the liquids. It seemed that the combination of unbalanced motion resistance and Laplace pressure drove directional transport of liquids. When patterned on elastic substrates, mechanical stretching could change characteristic geometric parameters of the patterns and thereby switch the direction of liquid transport. Thus, this study may not only offer a low-cost and scalable solution to achieve long-distance surface transport of liquids, but also provide an endurable type of Vshape patterns for directional liquid transport. The responsiveness to liquids and strain offered extra flexibility of switching liquid transport directions essential in liquid droplet separation open-channel microfluidics.

#### Experimental section

#### Fabrication of patterned surfaces

Asymmetric functional surfaces are fabricated via a direct-inkwriting printer (Adventure-3D-LB-Printer-0100, Adventure Tech Inc.). DOWSIL SE 1700 Clear base and the catalyst were mixed at a mass ratio of 10/1 and stirred for 15 min. The prepared mixture was introduced into an extrusion syringe and subjected to centrifugal treatment at 3000 rpm for 5 min to remove trapped air bubbles. Subsequently, the resulting silicone ink was deposited onto a pre-cleaned glass slide through a nozzle (inner diameter is 340 μm) along a preset trajectory that was designed using CAD software, and the extrusion pressure was maintained at 0.5 MPa. The distance between the nozzle tip and substrate is about 200  $\mu m$  and the printing velocity is 2 mm s<sup>-1</sup>. After printing, the surface was placed on a hot plate and cured at 85 °C for 1 h.

#### **Fabrication of elastic surfaces**

Polydimethylsiloxane (PDMS, DOWSIL 184 silicone elastomer) was used to print the soft surface. PDMS and the curing agent were mixed at a mass ratio of 10/1, stirred for 10 min and degassed in a vacuum oven for 30 min. The uncured PDMS mixture was coated on the cleaned glass substrates by using a spin coater (KW-4T, IMECAS, Beijing, China) with a rotational speed of 500 rpm for 30 s, and then heated on a hot plate at 75  $^{\circ}$ C for 1 h to fabricate the substrate. The PDMS ink was introduced into an extrusion syringe and degassed in a 45 °C vacuum

oven for 45 min to remove trapped air bubbles and improve the viscosity of ink. Then the precured PDMS ink was deposited onto the substrates through a nozzle (25G, inner diameter is 260 μm) along a preset trajectory, and the extrusion pressure was maintained at 0.3 MPa. The distance between the nozzle tip and substrate is about 150  $\mu$ m and the printing velocity is 2 mm s<sup>-1</sup>. After printing, the surface was placed on a hot plate and cured at 75 °C for 1 h and demolded from the glass.

#### Characterization

Water-ethanol mixtures with varied mass fractions (dved by using water-soluble dyes such as aniline blue) were injected into the center of the channel through a glass capillary that connected to a micro injector (RSP01-BG, RISTRON Inc.) with a constant injection velocity of 10  $\mu$ L s<sup>-1</sup>. The liquid transport behavior was monitored by using a digital camera (EOS800D, Canon) at 50 fps.

#### **Author contributions**

The study was conceptualized by C. Li and Y. Zhang. The methodology was developed by Y. Zhang, D. Pei, and M. Li. The investigation was carried out by Y. Zhang. Visualization was done by Y. Zhang. and C. Li. C. Li supervised the project. All authors contributed to the discussion. The original draft was written by Y. Zhang, with review and editing contributions from Y. Zhang, M. Li and C. Li.

#### Conflicts of interest

The authors declare no conflict of interest.

### Data availability

All data supporting the findings of this study are available within the paper and its supplementary information (SI). Supplementary information: surface tension, contact angles, durability test, effect of vertex radius R, surface morphology and liquid transport state after stretching. See DOI: https://doi.org/ 10.1039/d5ta05588a.

### Acknowledgements

The National Natural Science Foundation of China (No. 52173270, 22275204 and 22075307), Shandong "Taishan Scholars Program" & "Taishan Youth Scholars Program" projects (No. ZR2021YQ40, ZR2020ZD33 and ZR2020KE025) and project ZR2024QE188 supported by the Shandong Provincial Natural Science Foundation, Youth Innovation Promotion Association CAS (No. 2022209) and project of QIBEBT/SEI/ QNESL (No. S202303) are kindly acknowledged for financial support.

#### Notes and references

1 J. Ju, H. Bai, Y. Zheng, T. Zhao, R. Fang and L. Jiang, Nat. commun., 2012, 3, 1247.

- 2 P. Comanns, G. Buchberger, A. Buchsbaum, R. Baumgartner, A. Kogler, S. Bauer and W. Baumgartner, *J. R. Soc. Interface*, 2015, **12**, 20150415.
- 3 A. R. Parker and C. R. Lawrence, Nature, 2001, 414, 33-34.
- 4 H. Chen, P. Zhang, L. Zhang, H. Liu, Y. Jiang, D. Zhang, Z. Han and L. Jiang, *Nature*, 2016, 532, 85–89.
- 5 C. Liu, Y. Zheng and L. Jiang, ACS Nano, 2014, 8, 1321-1329.
- 6 X. Liu, B. Li, Z. Gu and K. Zhou, Small, 2023, 19, e2207640.
- 7 L. Shang, Y. Yu, W. Gao, Y. Wang, L. Qu, Z. Zhao, R. Chai and Y. Zhao, Adv. Funct. Mater., 2018, 28, 1705802.
- 8 X. Han, S. Tan, R. Jin, L. Jiang and L. Heng, *J. Am. Chem. Soc.*, 2023, **145**, 6420–6427.
- J. Li, X. Zhou, R. Tao, H. Zheng and Z. Wang, *Langmuir*, 2021, 37, 5059–5065.
- 10 Z. Ye, G. Zhao, Q. Tong, X. Wang, H. Su, H. Bai, K. Liu and M. Cao, J. Mater. Chem. A, 2024, 12, 16373.
- 11 M. Li, J. Hao, H. Bai, X. Wang, Z. Li and M. Cao, *ACS Appl. Mater. Interfaces*, 2023, **15**, 19773–19782.
- 12 Y. Chen, K. Li, S. Zhang, L. Qin, S. Deng, L. Ge, L. P. Xu, L. Ma, S. Wang and X. Zhang, ACS Nano, 2020, 14, 4654– 4661.
- 13 M. Zhang, L. Wang, Y. Hou, W. Shi, S. Feng and Y. Zheng, *Adv. Mater.*, 2015, 27, 5057–5062.
- 14 C. Lv, C. Chen, Y.-C. Chuang, F.-G. Tseng, Y. Yin, F. Grey and Q. Zheng, *Phys. Rev. Lett.*, 2014, **113**, 026101.
- 15 Y. Chen, D. Shi, X. Mai, L. Li, J. Gao, X. Chen, H.-X. Li and C.-P. Wong, *Microfluid. Nanofluid.*, 2017, 22.
- 16 R. W. Style, Y. Che, S. J. Park, B. M. Weon, J. H. Je, C. Hyland, G. K. German, M. P. Power, L. A. Wilen, J. S. Wettlaufer and E. R. Dufresne, *Proc. Natl. Acad. Sci. U. S. A.*, 2013, 110, 12541–12544.
- 17 J. Li, J. Li, J. Sun, S. Feng and Z. Wang, *Adv. Mater.*, 2019, **31**, e1806501.
- 18 Y. Cui, D. Li and H. Bai, *Ind. Eng. Chem. Res.*, 2017, **56**, 4887–4897.
- 19 L. Yang, W. Li, J. Lian, H. Zhu, Q. Deng, Y. Zhang, J. Li, X. Yin and L. Wang, *Science*, 2024, 384, 1344–1349.

- 20 Y. Guo, Y. Luo, L. Liu, C. Ma, C. Liu, J. Wang, X. Gao, X. Yao and J. Ju, J. Mater. Chem. A, 2023, 11, 12080.
- 21 Z. Li, D. Zhang, D. Wang, L. Zhang, L. Feng and X. Zhang, ACS Appl. Mater. Interfaces, 2019, 11, 48505–48511.
- 22 X. Chen, X. Li, P. Zuo, M. Liang, X. Li, C. Xu, Y. Yuan and S. Wang, *ACS Appl. Mater. Interfaces*, 2021, **13**, 13781–13791.
- 23 Y. Zhu, Y. Zhang, Z. Zhao, L. Zhang, X. Liu and H. Chen, Surf. Interfaces, 2024, 54, 105111.
- 24 Z. Cui, L. Xiao, Y. Li, Y. Zhang, G. Li, H. Bai, X. Tang, M. Zhou, J. Fang, L. Guo, S. Liu, C. Xiao and M. Cao, J. Mater. Chem. A, 2021, 9, 9719–9728.
- 25 S. Feng, P. Zhu, H. Zheng, H. Zhan, C. Chen, J. Li, L. Wang, X. Yao, Y. Liu ang and Z. Wang, *Science*, 2021, 373, 1344– 1348.
- 26 X. Liu, M. Gao, B. Li, R. Liu, Z. Chong, Z. Gu and K. Zhou, Adv. Mater., 2024, 36, e2310797.
- 27 C. Wei, Y. Zong and Y. Jiang, ACS Appl. Mater. Interfaces, 2023, 15, 24989–24998.
- 28 C. Wei, O. Gendelman and Y. Jiang, ACS Nano, 2025, 19, 7317–7326.
- 29 Q. An, J. Wang, F. Zhao, P. Li and L. Wang, Soft Matter, 2021, 17, 8153–8159.
- 30 Y. Zhang, Y. Gan, L. Zhang, Y. Guo, Y. Wang, Z. Wang, X. Liu, P. Zhang, T. Ran, L. Jiang and H. Chen, Adv. Mater. Interfaces, 2022, 9, 2102547.
- 31 J. Berthier, K. A. Brakke and E. Berthier, *Microfluid. Nanofluid.*, 2013, **16**, 779–785.
- 32 F. F. Ouali, G. McHale, H. Javed, C. Trabi, N. J. Shirtcliffe and M. I. Newton, *Microfluid. Nanofluid.*, 2013, **15**, 309–326.
- 33 W. J. Hyun, S. Kumar, L. F. Francis and C. D. Frisbie, *Appl. Phys. Lett.*, 2018, 113, 193701.
- 34 X. Li, J. Li and G. Dong, ACS Appl. Mater. Interfaces, 2020, 12, 5113–5119.
- 35 H. Geng, H. Bai, Y. Fan, S. Wang, T. Ba, C. Yu, M. Cao and L. Jiang, *Mater. Horiz.*, 2018, 5, 303–308.